NANO · MICRO small
www.small-journal.com

Check for updates

Wearable and Ultrasensitive Strain Sensor Based on High-Quality GaN pn Junction Microwire Arrays

Shiduo Cheng, Sancan Han, Ziyang Cao, Chenchao Xu, Xiaosheng Fang, and Xianying Wang**

With the rapid growth in wearable electronics sensing devices, flexible sensing devices that monitor the human body have shown great promise in personalized healthcare. In the study, high-quality GaN pn junction microwire arrays with different aspect ratios and large-area uniformity are fabricated through an easy, repeatable fabrication process. The piezoelectric coefficient (d_{33}) of GaN pn junction microwire arrays increases from 7.23 to 14.46 pm V^{-1} with the increasing of the aspect ratio, which is several times higher than that of GaN bulk material. Furthermore, flexible ultrasensitive strain sensor based on GaN microwires with the highest d_{33} is demonstrated to achieve the maximum open circuit voltage of 10.4 V, and presents excellent durability with stable output signals over 10 000 cycles with a response time of 50 ms. As a flexible and wearable sensor attached to the human skin, the GaN microwire pn junction arrays with such a high degree of uniformity can precisely monitor subtle human pulse and motions, which show great promise in future personalized healthcare.

1. Introduction

Wearable electronics that can be integrated into human bodies providing real-time detection of healthcare and environment parameters are attracting more and more attention. A great number of wearable and flexible sensors have been developed for various functions in recent years, such as temperature sensor, humidity sensor, strain sensor, and pH sensor.[1–6] Among these sensors, flexible strain sensors, which transduce mechanical stimuli into electrical counterparts, have been the major interest of many research teams because of the ubiquitous mechanical energy in the surroundings from human body motions even to air flow.[7–9] On the basis of different mechanisms, flexible strain sensors can be divided into several types including piezoresistivity, capacity, and piezoelectricity.[10–14] The piezoresistive strain sensors are unquestionably promising candidates for wearable and real-time human motion-detecting devices,[15,16] and they can be sensitive enough for even 10 nm vibration,[17] but the piezoelectric sensors are more prospective for self-powered devices owing to the piezoelectric effect of materials, defined as the occurrence of polarization when the material is subjected to external stress as a result of the separation of the positive and negative gravity centers of the molecules. Lead zirconate titanate (PZT) and polyvinylidene fluoride (PVDF) are the most commonly used piezoelectric mediums for piezoelectric sensors due to their high piezoelectric coefficients (d_{33}).[18–21] However, the toxic lead component in PZT and the high impedance of PVDF have limited their applications in wearable piezoelectric devices.[22,23] In this regard, semiconductor-based piezoelectric strain sensors represented by zinc oxide (ZnO) and GaN have been extensively studied as a result of their mechanical and chemical stability as well as environmental and biological compatibility.[24–28]

In addition to the above advantages of the semiconductor, GaN exhibits merits of easy control of carrier concentration doping and higher stability compared to ZnO, while internal free carriers reduce the output of the device by screening the piezoelectric polarization, which is called free carriers screening. Suppressing the free carriers screening is undoubtedly an effective approach to improve the piezoelectric performance of the devices.[27,29,30] Another method is replacing the bulk or film materials with nanowires (NWs) considering the superior mechanical properties, large aspect ratio, and high energy conversion efficiency of NWs as compared to bulk materials.[31–35] For instance, Kacimi et al. fabricated a flexible strain sensor exhibiting 2 V peak outputs with vertically aligned ultra-long GaN wires,[36] which required relatively longer GaN NW transfer to flexible substrate by doctor blading. Kang et al. improved the output of the GaN-based flexible devices through the formation of homojunction(p-type GaN film/n-type GaN film) and heterojunction(p-type NiO film/n-type GaN NWs) to suppress the free carriers screening;[22,37] however, more defects formed at the GaN NW/film interface because p-NiO layer was relatively hard to control during the growth. Therefore, an easy to control, cost-effective, and scalable fabrication method for GaN arrays with pn homojunctions is highly desirable for practical application.

S. D. Cheng, Dr. S. C. Han, Z. Y. Cao, C. C. Xu, Prof. X. Y. Wang
School of Materials Science and Engineering
University of Shanghai for Science and Technology
Shanghai 200093, P. R. China
E-mail: xianyingwang@usst.edu.cn

Prof. X. S. Fang
Department of Materials Science
Fudan University
Shanghai 200433, P. R. China
E-mail: xshfang@fudan.edu.cn

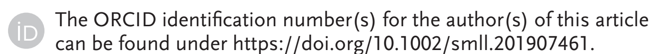
The ORCID identification number(s) for the author(s) of this article can be found under https://doi.org/10.1002/smll.201907461.

DOI: 10.1002/smll.201907461

© 2020 WILEY-VCH Verlag GmbH & Co. KGaA, Weinheim

Herein, high-quality GaN pn junction microwire arrays with different aspect ratios and large-area uniformity are fabricated through a top-down technique combined with lithography, dry etching, and wet etching method. Different diameters of 1.60, 1.29, 0.98, and 0.71 µm for GaN microwire arrays with the same heights of 3.0 µm were achieved, which were defined as H/D 1.9, H/D 2.3, H/D 3.1, and H/D 4.2, respectively, according to their aspect ratios (height/diameter). The piezoelectric coefficient (d_{33}^{eff}) of GaN microwire arrays with different aspect ratios was experimentally measured by piezoelectric force microscopy (PFM) and the effect of piezoelectric coefficient of GaN microwires increased from 7.23 to 14.46 pm V^{-1} with the increasing of the aspect ratio. Furthermore, the flexible strain sensor based on the GaN H/D 4.2 microwire arrays with the biggest piezoelectric coefficients was constructed. The piezoelectric voltage could be achieved from 2 mV to 10.4 V with the current of tens of nanoamperometer (nA), which may be ascribed to the suppressing of the free carriers screening due to the orderly pn junction in GaN microwire arrays. The wearable device based on the GaN microwires pn junction arrays with such a high degree of uniformity showed excellent durability with stable output signals over 10 000 cycles with a response time of 50 ms, which could precisely monitor subtle human pulse and motions.

2. Results and Discussion

The schematic of the preparation process of GaN microwire arrays is shown in **Figure 1**a. The GaN microwire arrays were prepared through a top-down technique combined with lithography, dry etching, and wet etching. The diameter of the GaN microwires would be smaller than designed after the dry etching and wet etching. As shown in Figure 1b,c, the diameter of GaN wires is ≈1.88 µm after dry etching, meanwhile the diameter went down to ≈1.6 µm because the wet-etching process was taken by KOH solution for sidewall smoothing. The sidewalls of the GaN microwire arrays are relatively rough due to the mechanical damage during the Cl_2 dry-etching process, resulting in the existence of some opening bonds on the crystal surface atoms, which are easy to bond with OH^- molecules in KOH solution to achieve the wet etching.

The scanning electron microscopy (SEM) images of GaN microwire arrays are shown in **Figure 2**a–d. As can be seen, high-quality GaN microwire arrays with different aspect ratios are fabricated according to the top-down method, which shows higher large-area uniformity than the bottom-up method.[36,37] Besides, the quality of the pn homojunctions GaN is much easier to control by the top-down method, profiting from the less defects in the interface during the growth of thin films. The diameters of GaN H/D 1.9, H/D 2.3, H/D 3.1, and H/D 4.2 are ≈1.60, ≈1.29, ≈0.98, and ≈0.71 µm, respectively. The height of the four diameters of GaN microwires are all ≈3.0 µm, which is evidenced by Figure 2d and Figure S1, Supporting Information. Figure 2e shows the Raman spectroscopy of GaN microwire arrays with different aspect ratios. The phonon frequencies of E_2 (high) mode of GaN microwire arrays with different aspect ratios are all located in ≈571.1 cm. The width of these peaks for GaN microwire arrays is almost the same, indicating that the crystallinity of the GaN with different aspect ratios maintained constant.[38] The room-temperature

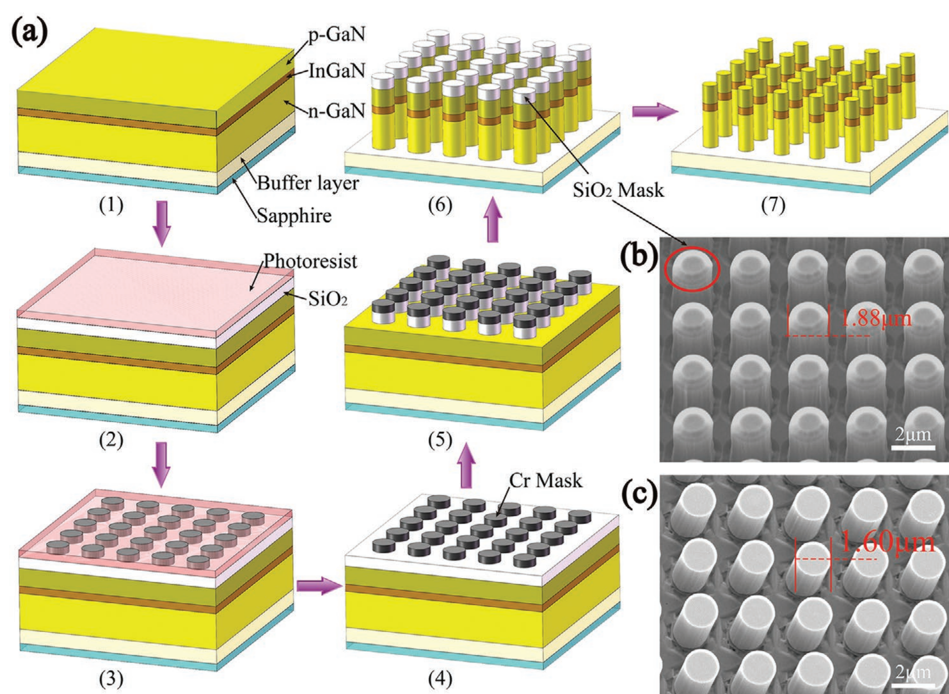

Figure 1. a) Schematic illustration of the preparation process for GaN microwires: 1) GaN epitaxial layer grown on a sapphire substrate; 2) SiO_2 layer depositing and photoresist spin-coating; 3) Metalization on the patterned photoresist; 4) lift-off of photoresist; 5) selective etching of the SiO_2 layer; 6) dry etching of GaN; and 7) wet-etching of GaN and SiO_2 masks removal. SEM images of GaN microwire arrays: b) before and c) after wet-etching and SiO_2 masks removal.

© 2020 WILEY-VCH Verlag GmbH & Co. KGaA, Weinheim

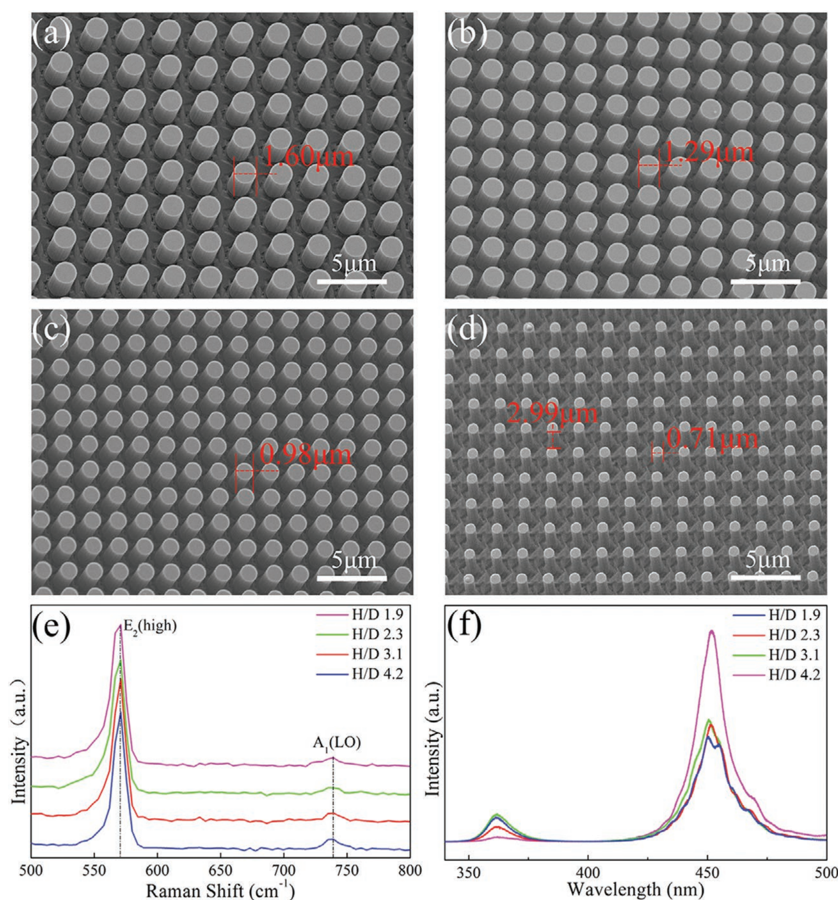

Figure 2. SEM images of GaN microwire arrays with different diameters: a) H/D 1.9; b) H/D 2.3; c) H/D 3.1; d) H/D 4.2; e) Raman spectroscopy; and f) room temperature PL of GaN microwire arrays with different aspect ratios.

photoluminescence (PL) spectroscopy of GaN microwire arrays with different aspect ratios is shown in Figure 2f. Two emission peaks located at ≈361.46 and ≈451.8 nm respond to GaN and InGaN, respectively, and the full width at half maximum of the two peaks are ≈11 and ≈15 nm. The unchangeable narrow peaks evidenced the high crystal quality of the GaN microwire arrays with different aspect ratios.[39,40]

Piezoelectric coefficient is the relation between the strain and electric field intensity, where the strain is detected under a given potential. The effect of the diameter for GaN microwire arrays on piezoelectric coefficient (d_{33}) was investigated by atomic force microscope (AFM) by a two-step scanning. The GaN microwire arrays were first scanned by AFM under alternating contact mode for topography (**Figure 3**a). The samples were scanned again under PFM mode. During PFM scanning, the Pt/Ir-coated conductive tip was applied with 1 V alternating current (AC) bias, and the top of the GaN microwire would deform in turn in response to the AC voltage on the tip. The alternating deformation can be measured as a vibration amplitude (Figure 3b,c). The detailed operation process and results of PFM measurements are shown in Figure S2, Supporting Information. In PFM mode, the relation between the AC bias and the amplitude is defined as

$$A = d_{33}^{\mathrm{eff}} \cdot V_{\mathrm{ac}} \qquad (1)$$

where A is the vibration amplitude detected by the tip, that is called PFM amplitude, V_{ac} is the AC bias applied on the tip, and d_{33}^{eff} is the effective piezoelectric coefficient of the sample that depends on the contribution from other tensor elements and on the crystallographic and real space orientation of the piezo material.

Figure 3d shows the PFM amplitudes of different size of GaN microwires under the increasing tip bias from 1 to 5 V. The effective piezoelectric coefficient d_{33}^{eff} equals to the slope of the fitting line. In **Table 1**, the calculated slopes for four different sample of H/D 1.9, H/D 2.3, H/D 3.1, and H/D 4.2 are 7.23, 9.19, 10.08, and 14.46 pm V^{-1}, respectively, which are almost several times higher than that of GaN bulk materials (3.7 pm V^{-1}),[41] indicating the enhanced piezoelectric properties. The larger d_{33}^{eff} means more strain rate along *c*-axis under the same AC bias on the tip, meaning better piezoelectric property of GaN microwire arrays. It can be seen that the d_{33}^{eff} of GaN microwire arrays increases with the decreasing diameter, which may be attributed to the volume contraction induced by the residual surface stress. The volume contraction rate from the residual surface stress plays a key role in piezoelectric coefficient, and the H/D 4.2 microwire arrays own larger specific surface and residual surface stress, resulting in a higher volume contraction rate as well as larger piezoelectric coefficient.[42,43] As shown in Figure S3, Supporting Information, conductive AFM has also been taken to test their piezoelectric performance. The piezoelectric voltages of GaN microwires with different aspect ratios are presented in Figure S4, Supporting Information. Meanwhile, the piezoelectric voltages of GaN microwires with different aspect ratios from the conductive atomic force microscope are presented in Table S1, Supporting Information. In comparison, the H/D 4.2 microwire arrays would generate a higher voltage with the same force. Both the PFM and conductive AFM results have shown that GaN H/D 4.2 has the best piezoelectric performance.

GaN H/D 4.2 microwire arrays were selected to design the flexible and wearable strain sensor. The fabrication process of the flexible strain sensor is schematically shown in **Figure 4**. The GaN microwires were first completely covered by a spin-coated polydimethylsiloxane (PDMS) layer, and the tops of microwires were exposed by CF_4/O_2 etching (Figure 4b; Figure S5, Supporting Information). The GaN microwires were then coated with metal electrode on the exposed tops (Figure 4c). PET thin film with an adhesive surface was selected as the flexible substrate, and then conductive silver adhesives were coated on part of the PET adhesive surface (red area in Figure 4d). The metal electrode of GaN microwires bonded to the part of silver adhesives on the PET and left silver adhesives was used for wire connecting. After the metal electrode, GaN microwires were bonded to flexible substrate, the sapphire substrate was

© 2020 WILEY-VCH Verlag GmbH & Co. KGaA, Weinheim

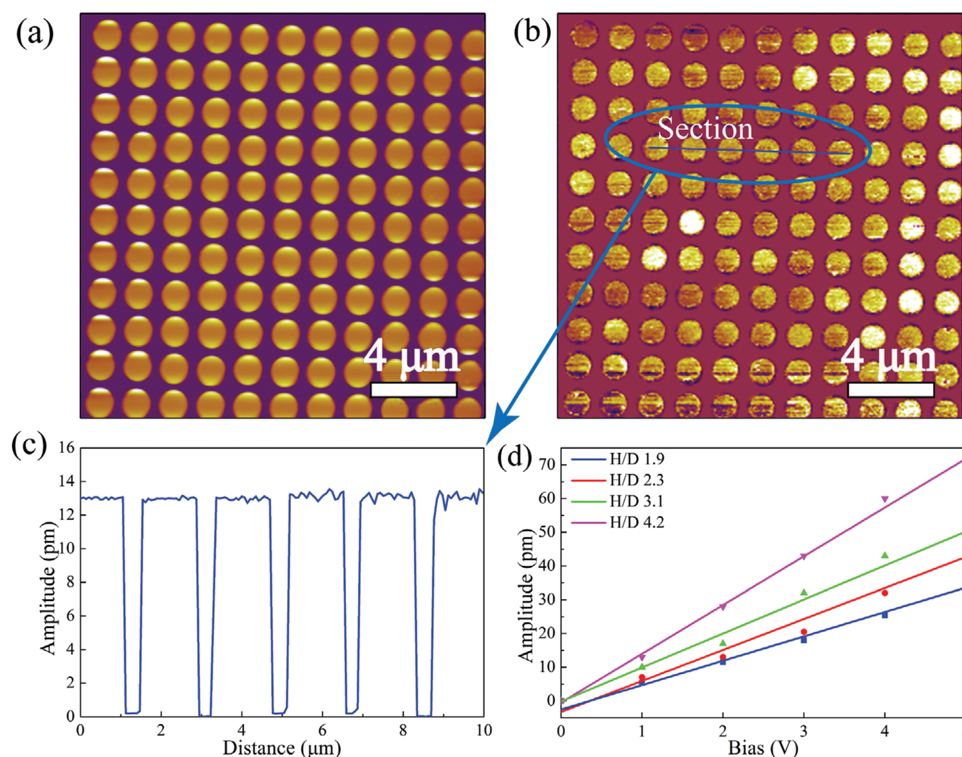

Figure 3. a) AFM topography and b) PFM amplitude of H/D 4.2. c) Section of the PFM amplitude of H/D 4.2; d) PFM amplitude of GaN microwire arrays with different diameters under different tip bias.

removed by laser lift-off (Figure 4e; Figure S6, Supporting Information), and the top electrode was deposited at last (Figure 4f). As shown in **Figure 5**a, the current–voltage (I–V) of GaN-based flexible strain sensor was carried out; the inset of Figure 5a is the photograph of GaN-based flexible strain sensor. Typical I–V curve of pn junction rectification can be observed with the built-in electric field of ≈2.52 V. Junction current screening originating from the reverse leakage current is the dominating screening mechanism in GaN pn junction-based piezoelectric device. The current flowing through the pn junction would decrease the output by screening the piezoelectric polarization, hence a low reverse leakage current is vital to the pn junction piezoelectric sensor.[44] The reverse leakage current in the I–V curve is 78 nA, evidencing the low junction current screening in the flexible strain sensor. The flexible strain senor was first attached to the wrist by medical proof fabric and characterized by detecting human pulse. Figure 5b shows the voltage signals of pulse detecting before and after 1000 m running. The peak of generated potential in normal state before 1000 m running is 1.87 mV with the frequency of 78 beats per minute and 2.25 mV potential with 114 beats per minute frequency after 1000 m running. The increase of both voltage and frequency indicates that the flexible strain sensor can precisely detect the heart rate change as well as the beat strength.

Table 1. Effective piezoelectric coefficients (d_{33}^{eff}) of GaN microwires with different aspect ratios.

Sample	H/D 1.9	H/D 2.3	H/D 3.1	H/D 4.2
Diameter [µm]	1.60	1.29	0.98	0.71
d_{33}^{eff} [pm V^{-1}]	7.23	9.19	10.08	14.46

The voltage and current were successfully measured when the flexible strain sensor was bent by finger force of ≈180 mN force, ≈90° bent angle, which is demonstrated in Figure 5c,d. The piezoelectric voltage generated by finger bending is ≈2.62 V with the current of 32.5 nA. Figure 5e,f depicts the magnified views of the voltage and current in one cycle. The inset of Figure 5e is the real bend condition of the flexible sensor by finger force. As shown in Figure 5e, the voltage or current in one cycle can be divided into four parts, corresponding to the normal state, stress applying, stress holding, and stress releasing. Swift electric signal would occur with the response time of ≈50 ms after the stress was applied. The piezoelectric voltage would be screened by the free carriers and junction current in the GaN microwire arrays. Similarly, an inverse voltage would occur and disappear once the stress was released. The above results evidenced the successful fabrication of flexible and ultrasensitive flexible strain sensor based on the GaN microwire arrays.

To discuss the detailed generating and decaying behavior of the electric signal in response to the compress, the mechanism during the development of piezoelectric charges is shown in **Figure 6**. Figure 6a is the original state of GaN microwire arrays before the application of the stress. Then opposite piezoelectric charges occur instantly at the two ends of the GaN microwire arrays once the stress is applied (Figure 6b), generally the piezoelectric charges will be swiftly screened

 © 2020 WILEY-VCH Verlag GmbH & Co. KGaA, Weinheim

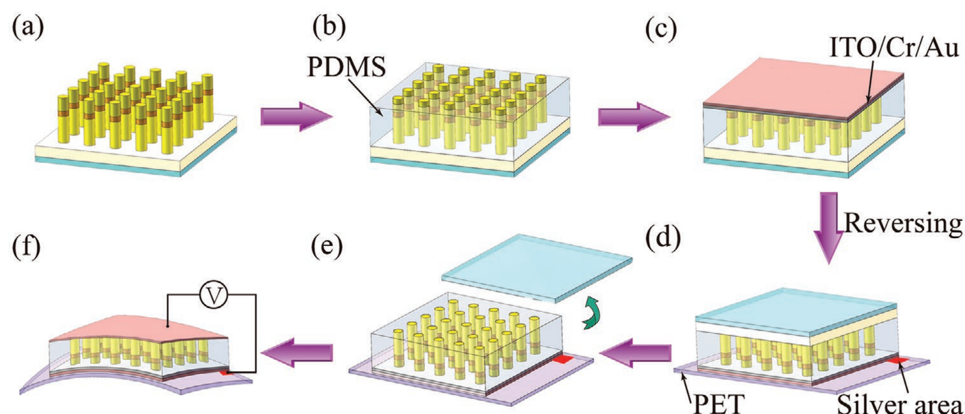

Figure 4. Schematic illustration of the fabrication process of the flexible strain sensor: a) GaN microwire arrays on sapphire substrate; b) PDMS spin-coating and tops exposing; c) electrode and laser block layer depositing; d) flexible substrate bonding; e) sapphire removal by laser lift-off; f) top electrode depositing.

Figure 5. a) I–V measurements of the flexible strain sensor, the inset shows the photograph of the flexible strain sensor. b) Human pulse signals detected by the flexible strain sensor in normal circumstances and after 1000 m running. c) Piezoelectric voltage and current; d) by finger force bending. e) Magnified view of piezoelectric voltage and f) the current for one cycle; the inset of (e) shows the photograph of the flexible strain sensor bent by finger force.

© 2020 WILEY-VCH Verlag GmbH & Co. KGaA, Weinheim

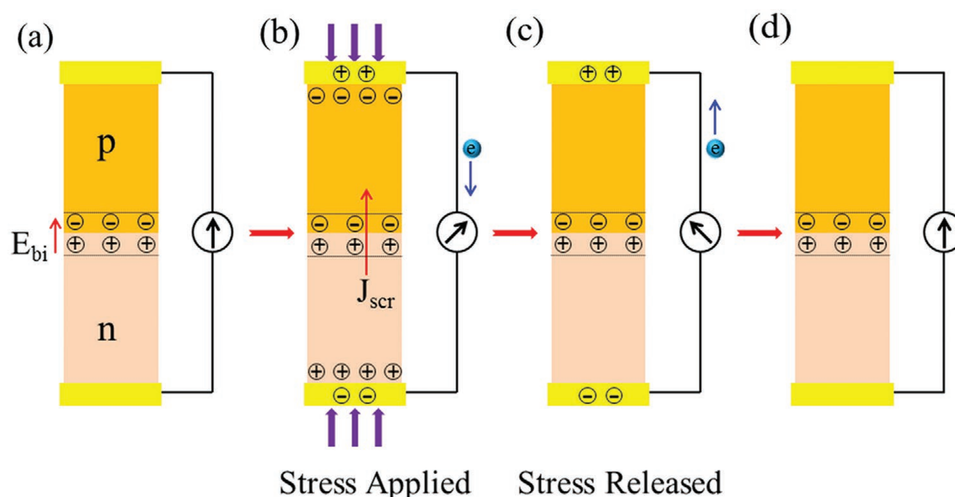

Figure 6. Time evolution of the signal illustrating the mechanism of the flexible strain sensor: a) Normal condition before the stress applied; b) Piezoelectric potential occurs as the stress is applied and the external electrons driven by the piezoelectric potential, causing a positive signal; c) Piezoelectric potential disappears as the stress is released and the electrons flow back, causing a negative signal; d) Recover to normal conditions again.

by the internal free carriers due to the semiconductor nature of GaN. Here, the free carriers screening is prevented by the built-in electric field within the pn junctions and the charges can be accumulated for higher voltage signal. In pn junction, the decaying of piezoelectric charges can be attributed to the following two reasons: the internal screening by the junction current (J_{scr}) and the electrons flow through the external circuit. Herein, high quality of pn junction contributes to negligible junction current screening, hence the external electrons flow is the main reason for the signal decaying, resulting in a detected voltage pulse. The piezoelectric charges would disappear once the stress is released and the accumulated charges on the electrodes flow back to the original state, resulting in an opposite signal (Figure 6c,d).

A further evaluation of the output voltage was characterized when the flexible strain sensor was stuck on the inner side of elbow joint by adhesive tape with different bent angle in cycles; the bent angle could be controlled by muscle memory. As shown in **Figure 7**a, the piezoelectric voltages are ≈1.42, ≈2.51, and ≈4.25 V with the increasing bent angle of arm of about ≈30°, ≈75°, and ≈120°. The higher piezoelectric output of the flexible strain sensor is generated with the increasing of bent angle,

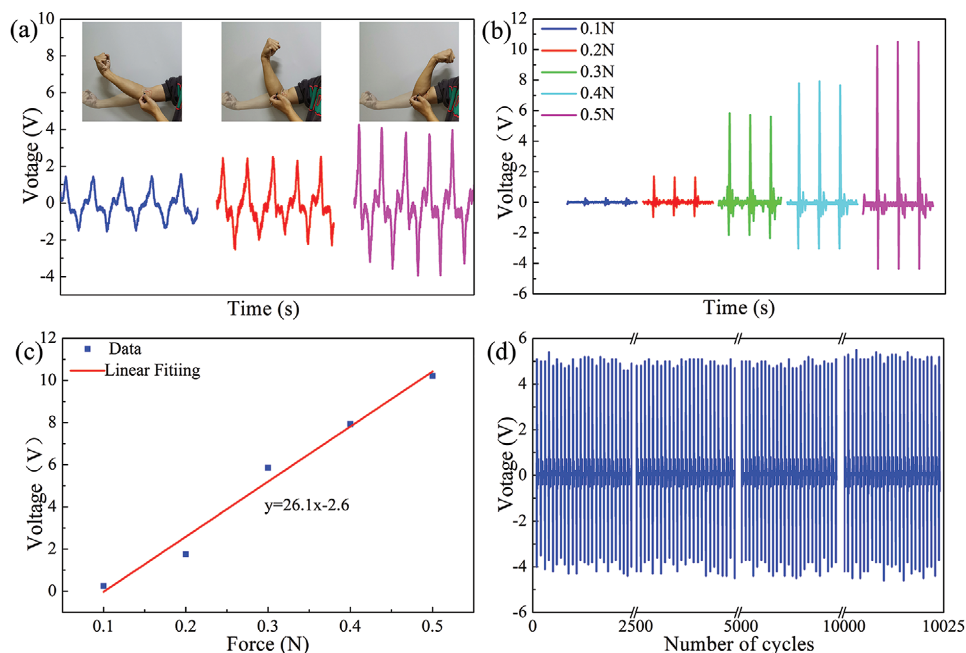

Figure 7. a) Voltages by arm bending to different angel; b) voltages by periodically punching with different force; c) the linear relation between the output voltage and punching force; and d) more than 10 000 cycles of periodicity punching at the frequency of 4 Hz illustrating the durability of the flexible strain sensor.

© 2020 WILEY-VCH Verlag GmbH & Co. KGaA, Weinheim

which can be explained by higher compress stress in the PET substrate as well as larger deformation of GaN microwire arrays, evidencing the potential of the flexible strain sensor in detecting arm motion. Nevertheless, the piezoelectric performance of the flexible strain sensor is still restricted, because the mechanical energy has been partly converted into the elastic potential energy, which can be explained by the mechanical energy absorption of the flexible substrate and PDMS layer under bending condition. An effective way of improving the piezoelectric performance by reducing the conversion of the elastic potential energy should be introduced to assure that the applied stress can deform the GaN microwires to the maximum extent, which could achieve the highest piezoelectric potential along *c*-axis. Hence, an electromagnetic was employed as the periodic strength source to further evaluate the piezoelectricity of the flexible strain sensor, in which vertical punching was applied in the flexible strain sensor. Figure S7a, Supporting Information, is the photograph of electromagnetic punch; the part in the red cycle is driven by changeable voltage and can periodically hit the flexible strain sensor at a given force and frequency.

The piezoelectric voltage generated under the changeable strength is shown in Figure 7b. It can be seen that the piezoelectric voltage rises with the increasing vertical force from 0.1 to 0.5 N by electromagnetic punch. The linear relation between the piezoelectric voltage and the vertical force is shown in Figure 7c. The slope of the fitting line is ≈26.1 V N^{-1}, evidencing the remarkable signal correspondence of the flexible strain sensor. As shown in the curves in Figure S7b, Supporting Information, the flexible strain sensor can generate 10.4 V voltage under vertical force of 0.5 N, which is more than twice of that under bending, suggesting that the vertical stress is much more efficient than bending. The flexible strain sensor was vertically hit by the electromagnetic punch with the given frequency of 4 Hz for 10 000 cycles to evaluate the stability of the device. The highly uniform and stable potential output of the flexible strain sensor after 10 000 times cycle are shown in Figure 7d, evidencing the durability of the flexible strain sensor, which shows great promise in practical implementation in wearable sensing technologies.

3. Conclusions

In summary, patterned and uniform GaN microwire arrays with different aspect ratios have been obtained through a top-down method. The effect of aspect ratio of GaN microwire arrays on piezoelectric coefficient (d_{33}) has been successfully investigated by experimental measurements. The GaN microwires possess much higher d_{33} than bulk materials, and d_{33} of the GaN microwires with different aspect ratios increases from 7.23 to 14.46 pm V^{-1} with the decreasing of diameter, which is consistent with the reported theoretical simulation. The GaN H/D 4.2 with the highest d_{33} was selected for the fabrication of the flexible sensor. The flexible strain sensor based on GaN H/D 4.2 can precisely detect the change of heart rate as well as the beat strength with the output voltage of 2 mV, and it can also be used for sensing arm bending with the output voltage of 4.25 V. However, these stimuli cannot fully deform the GaN microwires along *c*-axis, hence vertical punching was applied in the flexible strain sensor to achieve the highest piezoelectric voltage. The piezoelectric voltage generated by vertical punching is linear with the loading force with a 26.1 V N^{-1} slope. The maximum open circuit voltage reached 10.4 V under vertical force and the performance of the flexible strain sensor is stable after 10 000 times cycle. Above all, the flexible strain sensor based on GaN microwire arrays with such a degree of uniformity has a significant impact on wearable electronics.

4. Experimental Section

Preparation of High-Quality GaN Microwire Arrays: The GaN epitaxial layers were grown by metalorganic chemical vapor deposition. First, a buffer layer (2.8 µm thick) was grown on the sapphire substrate and then the n-GaN (2.5 µm thick), InGaN (100 nm thick), and p-GaN (600 nm thick) layers were grown in sequence. After the epitaxial growth, a SiO_2 layer (1 µm thick) was deposited on p-GaN surface by plasma-enhanced chemical vapor deposition. Next, a photoresist layer was spin-coated on the SiO_2 layer and then patterned by interferometric lithography. After the lithography process, a 150 nm thick Cr layer was deposited in the holes of photoresist layer and then the photoresist was removed by acetone to obtain Cr masks. The Cr masks can selectively protect the SiO_2 layer during the following CF_4/O_2 etching process for SiO_2 masks. After that, Cl_2 etching was taken to remove the GaN uncovered by SiO_2 masks so that GaN microwires with rough sidewall could be obtained, and the sidewall was smoothen by wet etching. The SiO_2 masks can also protect the top of the microwires during the wet-etching process. Finally, the SiO_2 masks were removed by buffered oxide etchant solution.

Fabrication Process of Flexible Strain Sensor: PDMS (Sylgard 184, Dow Corning) was spin-coated on the GaN microwire arrays at a speed of 5000 rpm for 300 s and then hardened at 125 °C for 10 min. Then the GaN microwire arrays were completely covered by PDMS and the CF_4/O_2 etching process was taken to expose the top of GaN microwire arrays. A 300 nm layer of indium tin oxide was deposited on the top of GaN microwire arrays. Next, a Cr/Au (20 nm/200 nm) layer was deposited on ITO as bottom electrode, which can also prevent unwanted penetration of the laser beam as a laser block layer. After the metal surface was contacted with a PET film with a sticky surface for bonding, the sapphire substrate was removed owing to the decomposition the buffer layer during the laser lift-off process. Another layer of Au was deposited as the top electrode at last.

Characterization: The morphology of GaN microwire arrays was characterized by SEM (TESCAN Mira3) and AFM (Cypher ES). The piezoelectric coefficient of the GaN microwire arrays with different aspect ratios was measured by PFM (Cypher ES). Raman spectra of GaN microwire arrays were examined by Raman spectrometer (WITec). PL spectroscopy of GaN microwire arrays was collected using LabRAM HR Evolution spectrometer (Horiba, France) with the exciting wavelength of 325 nm. The piezoelectric performance of flexible strain sensor was carried out by an oscilloscope (InfiniiVision MSO-X 2014A). Experiments with human subjects were carried out with the full, informed consent of the subjects, in accordance with all local laws and with the approval of all relevant ethics bodies.

Supporting Information

Supporting Information is available from the Wiley Online Library or from the author.

Acknowledgements

S.D.C. and S.C.H. contributed equally to this work. The authors greatly appreciate the financial supports from the National Natural Science

© 2020 WILEY-VCH Verlag GmbH & Co. KGaA, Weinheim

Foundation of China (51802195, 51702212), Science and Technology Commission of Shanghai Municipality (18511110600, 19ZR1435200), Innovation Program of Shanghai Municipal Education Commission (2019-01-07-00-07-E00015), Program of Shanghai Academic Research Leader (19XD1422900), and the Shanghai Sailing Program (17YF1412700).

Conflict of Interest

The authors declare no conflict of interest.

Keywords

flexible strain sensors, GaN microwires, piezoelectric coefficient, pn junction

Received: December 19, 2019
Revised: February 12, 2020
Published online:

[1] G. Liu, Q. Tan, H. Kou, L. Zhang, J. Wang, W. Lv, H. Dong, J. Xiong, *Sensors* **2018**, *18*, 1400.
[2] J. Wu, Y. M. Sun, Z. Wu, X. Li, N. Wang, K. Tao, G. P. Wang, *ACS Appl. Mater. Interfaces* **2019**, *11*, 4242.
[3] B. T. Li, G. Xiao, F. Liu, Y. Qiao, C. M. Li, Z. S. Lu, *J. Mater. Chem. C* **2018**, *6*, 4549.
[4] S. Cai, X. Xu, X. Wu, J. Chen, C. Zuo, X. S. Fang, *J. Mater. Chem. C* **2019**, *7*, 13097.
[5] S. Nakata, M. Shiomi, Y. Fujita, T. Arie, S. Akita, K. Takei, *Nat. Electron.* **2018**, *1*, 596.
[6] Q. Hua, J. Sun, H. Liu, R. Bao, R. Yu, J. Zhai, C. Pan, Z. L. Wang, *Nat. Commun.* **2018**, *9*, 244.
[7] Y. Z. Lei, T. M. Zhao, H. X. He, T. Y. Zhong, H. Y. Guan, L. L. Xing, B. D. Liu, X. Y. Xue, *Smart Mater. Struct.* **2019**, *28*, 105001.
[8] M. A. Johar, J. H. Kang, M. A. Hassan, S. W. Ryu, *Appl. Energy* **2018**, *222*, 781.
[9] T. Huang, P. He, R. R. Wang, S. W. Yang, J. Sun, X. M. Xie, G. Q. Ding, *Adv. Funct. Mater.* **2019**, *29*, 45.
[10] S. Chen, Y. J. Song, D. Y. Ding, Z. Ling, F. Xu, *Adv. Funct. Mater.* **2018**, *28*, 42.
[11] X. H. Liu, G. H. Su, Q. Q. Guo, C. H. Lu, T. Zhou, C. L. Zhou, X. X. Zhang, *Adv. Funct. Mater.* **2018**, *28*, 15.
[12] J. Qiu, X. Guo, R. Chu, S. Wang, W. Zeng, L. Qu, Y. Zhao, F. Yan, G. Xing, *ACS Appl. Mater. Interfaces* **2019**, *11*, 40716.
[13] H. Nesser, J. Grisolia, T. Alnasser, B. Viallet, L. Ressier, *Nanoscale* **2018**, *10*, 10479.
[14] T. Huang, S. Yang, P. He, J. Sun, S. Zhang, D. Li, Y. Meng, J. Zhou, H. Tang, J. Liang, G. Ding, X. Xie, *ACS Appl. Mater. Interfaces* **2018**, *10*, 30732.
[15] D. Cho, J. Park, J. Kim, T. Kim, J. Kim, I. Park, S. Jeon, *ACS Appl. Mater. Interfaces* **2017**, *9*, 17369.
[16] D. Cho, J. Park, T. Kim, S. Jeon, *J. Semicond.* **2019**, *40*, 111605.
[17] D. Kang, P. V. Pikhitsa, Y. W. Choi, C. Lee, S. S. Shin, L. Piao, B. Park, K.-Y. Suh, T.-I. Kim, M. Choi, *Nature* **2014**, *516*, 222.
[18] K. I. Park, J. H. Son, G. T. Hwang, C. K. Jeong, J. Ryu, M. Koo, I. Choi, S. H. Lee, M. Byun, Z. L. Wang, K. J. Lee, *Adv. Mater.* **2014**, *26*, 2514.
[19] C. F. Lu, S. Wu, B. W. Lu, Y. Y. Zhang, Y. K. Du, X. Feng, *J. Micromech. Microeng.* **2018**, *28*, 025010.
[20] G. Tian, W. L. Deng, Y. Y. Gao, D. Xiong, C. Yan, X. B. He, T. Yang, L. Jin, X. Chu, H. T. Zhang, W. Yan, W. Q. Yang, *Nano Energy* **2019**, *59*, 574.
[21] L. Jin, S. Ma, W. Deng, C. Yan, T. Yang, X. Chu, G. Tian, D. Xiong, J. Lu, W. Yang, *Nano Energy* **2018**, *50*, 632.
[22] J.-H. Kang, M. Ebaid, D. K. Jeong, J. K. Lee, S.-W. Ryu, *J. Mater. Chem. C* **2016**, *4*, 3337.
[23] J. H. Kang, D. K. Jeong, S. W. Ryu, *ACS Appl. Mater. Interfaces* **2017**, *9*, 10637.
[24] Z. L. Wang, J. Song, *Science* **2006**, *312*, 242.
[25] S. Xu, Y. Qin, C. Xu, Y. Wei, R. Yang, Z. L. Wang, *Nat. Nanotechnol.* **2010**, *5*, 366.
[26] G. Zhu, R. Yang, S. Wang, Z. L. Wang, *Nano Lett.* **2010**, *10*, 3151.
[27] C. H. Wang, W. S. Liao, Z. H. Lin, N. J. Ku, Y. C. Li, Y. C. Chen, Z. L. Wang, C. P. Liu, *Adv. Energy Mater.* **2014**, *4*, 16.
[28] Y. S. Zhou, R. Hinchet, Y. Yang, G. Ardila, R. Songmuang, F. Zhang, Y. Zhang, W. Han, K. Pradel, L. Montes, M. Mouis, Z. L. Wang, *Adv. Mater.* **2013**, *25*, 883.
[29] J. H. Kang, D. K. Jeong, J. S. Ha, J. K. Lee, S. W. Ryu, *Semicond. Sci. Technol.* **2017**, *32*, 025001.
[30] E. Lee, J. Park, M. Yim, S. Jeong, G. Yoon, *Appl. Phys. Lett.* **2014**, *104*, 21.
[31] D. C. Yang, Y. Qiu, Q. Y. Jiang, Z. S. Guo, W. B. Song, J. Xu, Y. Zong, Q. X. Feng, X. L. Sun, *Appl. Phys. Lett.* **2017**, *110*, 6.
[32] S. Salomon, J. Eymery, E. Pauliac-Vaujour, *Nanotechnology* **2014**, *25*, 375502.
[33] G. Zhu, A. C. Wang, Y. Liu, Y. Zhou, Z. L. Wang, *Nano Lett.* **2012**, *12*, 3086.
[34] S. Cai, X. J. Xu, W. Yang, J. X. Chen, X. S. Fang, *Adv. Mater.* **2019**, *31*, 1808138.
[35] W. G. Hu, K. Kalantar-Zadeh, K. Gupta, C. P. Liu, *MRS Bull.* **2018**, *43*, 936.
[36] A. El Kacimi, E. Pauliac-Vaujour, J. Eymery, *ACS Appl. Mater. Interfaces* **2018**, *10*, 4794.
[37] M. A. Johar, A. Waseem, M. A. Hassan, J. H. Kang, J. S. Ha, J. K. Lee, S. W. Ryu, *Acta Mater.* **2018**, *161*, 237.
[38] F. Demangeot, J. Frandon, M. Renucci, O. Briot, B. Gil, R.-L. Aulombard, *Solid State Commun.* **1996**, *100*, 207.
[39] S. J. Xu, W. Liu, M. F. Li, *Appl. Phys. Lett.* **2000**, *77*, 3376.
[40] D. Y. Song, M. Basavaraj, S. A. Nikishin, M. Holtz, V. Soukhoveev, A. Usikov, V. Dmitriev, *J. Appl. Phys.* **2006**, *100*, 113504.
[41] I. L. Guy, S. Muensit, E. M. Goldys, *Appl. Phys. Lett.* **1999**, *75*, 4133.
[42] R. J. Wang, C. Y. Wang, Y. T. Feng, C. Tang, *Nano Energy* **2018**, *53*, 906.
[43] H. P. Jiang, Y. J. Su, J. Zhu, H. M. Lu, X. K. Meng, *Nano Energy* **2018**, *45*, 359.
[44] J. I. Sohn, S. N. Cha, B. G. Song, S. Lee, S. M. Kim, J. Ku, H. J. Kim, Y. J. Park, B. L. Choi, Z. L. Wang, J. M. Kim, K. Kim, *Energy Environ. Sci.* **2013**, *6*, 97.

 © 2020 WILEY-VCH Verlag GmbH & Co. KGaA, Weinheim